Diffusion Tensor Imaging of the Substantia Nigra in Parkinson's Disease Revisited

Jason Langley,[1] Daniel E. Huddleston,[2] Michael Merritt,[1] Xiangchuan Chen,[1] Rebecca McMurray,[2] Michael Silver,[2] Stewart A. Factor,[2] and Xiaoping Hu[1]*

[1]*Wallace H. Coulter Department of Biomedical Engineering, Georgia Institute of Technology and Emory University, Atlanta, Georgia*
[2]*Department of Neurology, Emory University, Atlanta, Georgia*

Abstract: *Objective:* To analyze diffusion tensor imaging (DTI) data in the substantia nigra (SN) using a more consistent region of interest (ROI) defined by neuromelanin-sensitive MRI in order to assess Parkinson's disease (PD) related changes in diffusion characteristics in the SN. *Methods:* T_1-weighted and DTI data were obtained in a cohort of 37 subjects (17 control subjects and 20 subjects with PD). The subjects in the PD group were clinically diagnosed PD patients with an average Unified Parkinsonian Disease Rating Scale (UPDRS)-III score of 23.2 ± 9.3. DTI data were analyzed using SN ROIs defined by neuromelanin-sensitive MRI and, for comparison, with ROIs defined on T_2-weighted images ($b = 0$ images). *Results:* Compared with control subjects, significantly lower fractional anisotropy was observed in PD in the neuromelanin SN ROI but not in the ROI derived from the T_2-weighted image. This decrease was largest in the rostral and lateral portions of the neuromelanin volume, which were found to have more hypointensity in the T_2-weighted image and, presumably, higher iron content in the PD group. In addition, a larger decrease in fractional anisotropy was seen in the SN region of interest on the side contralateral to the side exhibiting more severe symptoms. These results indicate that the use of neuromelanin sensitive MRI to define the ROI in the SN for analyzing DTI data leads to more significant results, enhancing the robustness of DTI study and DTI based biomarkers of PD. *Hum Brain Mapp 37:2547–2556, 2016*.

Key words: Parkinson's disease; diffusion tensor imaging; substantia nigra; neuromelanin sensitive MRI

INTRODUCTION

Parkinson's disease (PD) is a neurodegenerative disorder characterized by a loss of motor learning and movement control. The catecholamine nuclei in the locus coeruleus and substantia nigra pars compacta (SNpc) degenerate before onset of PD symptoms. In the SNpc, the primary effect of PD is the loss of neuromelanin generating dopaminergic neurons [Fearnley and Lees, 1991] and other effects include an elevation of iron concentration

Contract grant sponsor: William N. and Bernice E. Bumpus Foundation Early Career Investigator Innovation Award; Contract grant number: BFIA 2011.3; Contract grant sponsor: NIH; Contract grant number: R01-CA169937; Contract grant sponsor: Udall Center for Excellence in Parkinson's Disease Research Pilot Award; Contract grant number: P50-NS071669; Contract grant sponsor: Michael J. Fox Foundation; Contract grant number: MJF 10854; Contract grant sponsor: NINDS Parkinson's Disease Biomarkers Program U18 Award; Contract grant number: U18 NS082143

*Correspondence to: Xiaoping P. Hu, The Wallace H. Coulter Department of Biomedical Engineering, Georgia Institute of Technology and Emory University, Health Sciences Research Building, 1760 Haygood Dr., Room W232, Atlanta, Georgia 30322. E-mail: xhu3@emory.edu

Received for publication 15 February 2016; Accepted 11 March 2016.

DOI: 10.1002/hbm.23192

Published online 29 March 2016 in Wiley Online Library (wileyonlinelibrary.com).

[Dexter et al., 1987, 1991; Wypijewska et al., 2010]. Various magnetic resonance imaging (MRI) techniques, such as diffusion tensor imaging (DTI), susceptibility weighted imaging [Rossi et al., 2010], quantitative susceptibility mapping [He et al., 2015], and neuromelanin sensitive MRI [Kashihara et al., 2011; Reimao et al., 2015b; Sasaki et al., 2006], have been used to delineate these changes in vivo.

Neuromelanin sensitive-MRI generates neuromelanin contrast using implicit magnetization transfer (MT) effects from the turbo spin echo (TSE) sequence [Kashihara et al., 2011; Reimao et al., 2015b; Sasaki et al., 2006] or explicit magnetization preparation pulses [Chen et al., 2014; Kitao et al., 2013; Ogisu et al., 2013]. Both approaches found disease related differences in the locus coeruleus and SNpc [Castellanos et al., 2015; Matsuura et al., 2013; Ogisu et al., 2013; Reimao et al., 2015a; Sasaki et al., 2006] although the MT-based approach was shown to generate more neuromelanin sensitive contrast in these structures than the TSE sequence [Chen et al., 2014]. In addition, several studies have found accordance between regions highlighted by neuromelanin-sensitive MRI and histological markers of neuromelanin [Keren et al., 2009, 2015; Kitao et al., 2013].

DTI allows for the assessment of tissue characteristics using measures such as the degree of diffusion anisotropy, as assessed with fractional anisotropy (FA), and the extent of diffusion, known as mean diffusion (MD). Several DTI studies have revealed lower FA in the SN in PD [Chan et al., 2007; Du et al., 2011; Peran et al., 2010; Vaillancourt et al., 2009]. Other studies found no differences in FA in the SN of PD patients [Aquino et al., 2014; Menke et al., 2009; Schwarz et al., 2013]. The discrepancy in results from different studies may be attributed to inconsistencies in SN ROIs used in the analysis of DTI data. In those studies, ROIs were manually drawn on T_2-weighted (T2w) spin echo ($b = 0$) images and could be highly subjective and variable. This variability has been a confounding factor in identifying potential PD biomarkers from DTI metrics [Schwarz et al., 2013].

The variability in SN ROIs defined based on T2w images can be partially attributed to differences in the extent of iron deposition in the SNpc among PD patients. In T2w images iron deposition presents themselves as hypointensity. However, iron deposition increases at different rates in PD patients, resulting in variability in the morphology and location of the hypointense region typically used to define SN ROIs for DTI data analysis. An example of such variability is illustrated in Figure 1.

In addition to the variability of SN ROIs defined in T2w images, these ROIs may not consistently capture the portion of SN containing neuromelanin. In normal subjects, SN volumes delineated by neuromelanin sensitive MRI and T2w images were found to be different not only in signal characteristics, but also spatially. As illustrated in Figure 2, SN regions detected by neuromelanin-sensitive MRI are located in a more caudal and medial position than the regions found in the T2w images [Langley et al., 2015]. In PD patients, due to variable iron deposition,

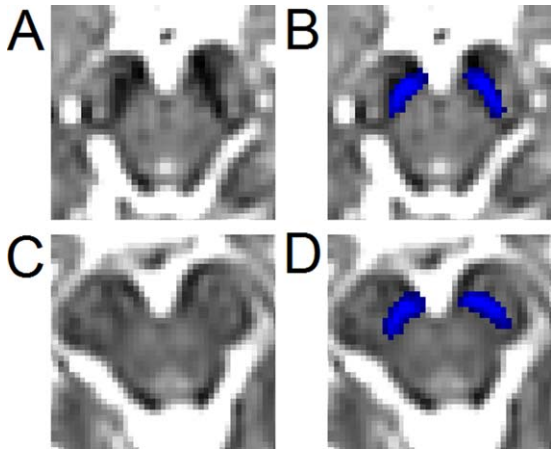

Figure 1.
Illustration of the inconsistency of SN hypointensity for two subjects with PD. Slices were placed four mm (two slices) below the red nucleus. The T2w hypointense SN for the first subject is shown in (**A**) with the NM SN (shown in blue) overlaid in (**B**). The T2w hypointense SN for the second subject is shown in (**C**) with the NM SN (shown in blue) overlaid in (**D**). Significant hypointensity is seen in (A) but is not present in the same region in (C). [Color figure can be viewed in the online issue, which is available at wileyonlinelibrary.com.]

ROIs defined on T2w images, in addition to its variability, likely do not consistently capture the portion of SN containing NM.

In this work, we avoid the problem of variability in SN ROIs used in previous studies by creating a standardized SNpc ROI, defined in neuromelanin-sensitive MRI images from healthy controls, and use this ROI to investigate differences in diffusion measures, namely MD and FA, in PD patients. We further compare these results to those from SN ROIs drawn on T2w images. Our results indicate that the ROIs defined using neuromelanin-sensitive MRI led to

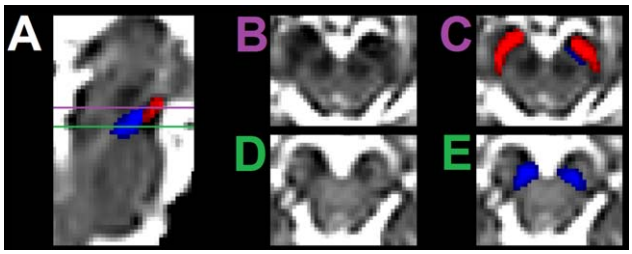

Figure 2.
Comparison of the spatial locations of the T2w SN volume (shown in red) and NM SN (shown in blue). A sagittal view of the brainstem from the $b = 0$ map is shown in (**A**). Axial views of the SN are shown in (**B**) and (**D**). The SN volumes overlaid on the axial images are shown in (**C**) and (**E**). [Color figure can be viewed in the online issue, which is available at wileyonlinelibrary.com.]

TABLE I. Demographic data for Parkinson's and control groups

	PD	CO	*P*
Subjects	20	17	—
Age (mean ± SD)	60.3 ± 8.4	70.8 ± 5.1	0.001
UPDRS-III motor score (mean ± SD)	23.2 ± 9.3	0.9 ± 1.4	$<10^{-5}$
MOCA (mean ± SD)	27.5 ± 2.3	26.7 ± 2.7	0.176

more significant differences between patients and normal controls.

METHODS

Subjects

A cohort of 37 subjects was scanned in the study, and all subjects gave written, IRB approved, informed consent in accordance with the Declaration of Helsinki in its currently applicable form. Demographic data for the cohort are summarized in Table I. The cohort was subdivided into a PD group consisting of 20 subjects (12 males and 8 females; aged 60.3 ± 8.4 years) and a control group consisting of 17 subjects (7 males and 10 females; aged 70.8 ± 5.1 years). The subjects in the PD group were clinically diagnosed PD patients with an average Unified Parkinsonian Disease Rating Scale (UPDRS)-III score of 23.2 ± 9.3. UPDRS-III motor examinations were performed to assess Parkinson's disease state in the ON medication condition. The Montreal Cognitive Assessment (MOCA) scores for the PD and control groups were 27.5 ± 2.3 and 26.7 ± 2.7, respectively. Sixteen subjects displayed lateralized impairment, 9 on the right side and 7 on the left side. Four subjects had both sides equally affected by PD.

Image Acquisition

All imaging data were acquired on two 3T MRI scanners (TRIO, Siemens Medical Solutions, Malvern, PA) at Emory University using a 12-channel receive only coil. Images from an MP-RAGE sequence (echo time (TE)/repetition time (TR)/inversion time = 3.02/2,600/800 ms, flip angle (FA) = 8°, voxel size = 1.0 × 1.0 × 1.0 mm^3) were used for registration from subject space to common space.

Diffusion MRI data were collected with a single-shot spin-echo, echo planar imaging sequence. A dual spin-echo technique combined with bipolar gradients was used to minimize eddy-current effects [Alexander et al., 1997]. Diffusion-weighting gradients were applied in 64 directions with a *b* value of 1,000 s/mm^2; TE/TR = 97/3,292 ms, FOV = 212 × 212 mm^2, matrix size of 106 × 106, voxel size = 2 × 2 × 2 mm^3, 64 slices with no gap, covering the entire brain. Two sets of diffusion-weighted images with phase-encoding directions of opposite polarity were acquired to correct for susceptibility distortion [Andersson et al., 2003]. For each diffusion-weighted acquisition, six images without diffusion weighting ($b = 0$ images) were also acquired with matching imaging parameters.

DTI Processing

Imaging data were analyzed with FSL [Jenkinson et al., 2002; Jenkinson and Smith, 2001; Smith et al., 2004] and MATLAB (The Mathworks, Natick, MA). Standard preprocessing steps were used to correct susceptibility induced distortions in the diffusion MR data. Diffusion MR data were first corrected for eddy-current distortion and for susceptibility distortion following the method of Andersson et al. [2003] as implemented in FSL. Next, skull stripping of the T_1-weighted image and susceptibility corrected $b = 0$ image was performed using the brain extraction tool in the FSL software package [Smith, 2002]. Finally,

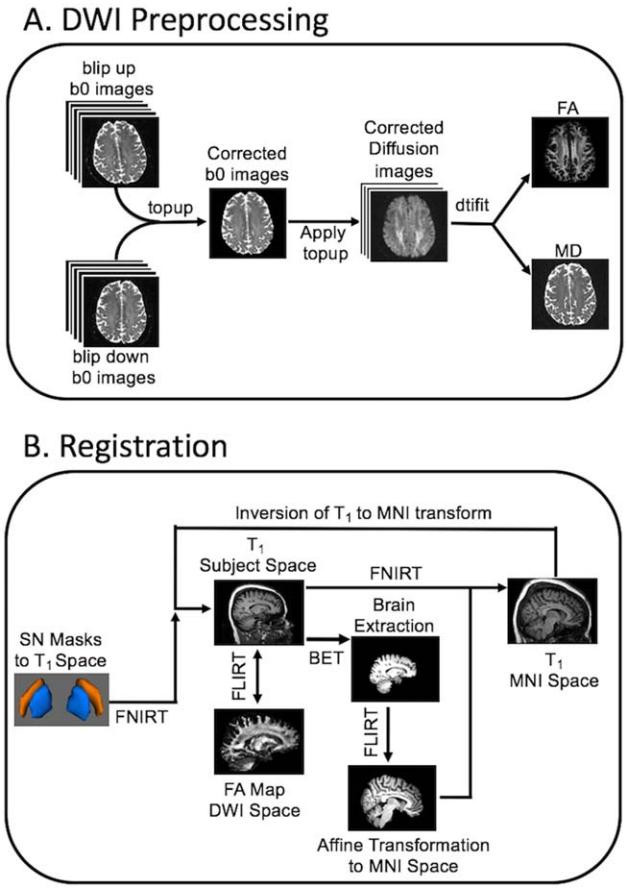

Figure 3.
Schematics illustrating the preprocessing procedure for DTI data (**A**) and registration from MNI to individual T_1 space (**B**). [Color figure can be viewed in the online issue, which is available at wileyonlinelibrary.com.]

measures derived from the diffusion MR data, including FA and MD, were calculated using the dtifit tool in FSL. This procedure is illustrated schematically in Figure 3A.

Creation of Neuromelanin SN Masks

Neuromelanin-sensitive MRI SN (NM SN) masks of a group of 11 normal subjects reported in a previous study [Langley et al., 2015] were transformed into the Montreal Neurological Institute (MNI) common space using FMRIB's Linear Image Registration Tool (FLIRT) and FMRIB's Nonlinear Image Registration Tool (FNIRT) tools in the FSL software package [Smith et al., 2004; Woolrich et al., 2009] as follows. First, a linear transformation from neuromelanin space to T_1 space was derived using FLIRT and individual SN masks were transformed to their respective T_1-weighted images using the aforementioned linear transformation. The resulting SN masks were transformed into common space by applying a nonlinear transform from T_1 space to common (MNI) space. The nonlinear transform from T_1 space to common space was derived using the following procedure: first, brain extracted images from the T_1-weighted MP-RAGE sequence were aligned with the MNI brain extracted image using an affine transformation (FLIRT). Second, a nonlinear transformation (FNIRT) was derived for transformation from individual subject T_1 space to common space.

After the transformation of each SN mask into MNI space, population masks for the NM SN were generated by averaging the left and right SN volumes across all subjects. The SN population mask was thresholded at a level of 0.6, corresponding to at least 60% of subjects sharing the voxel, and binarized. The resultant mask will be referred to as the NM SN mask.

Transformation of Neuromelanin SN Masks

The group NM SN mask, described in the previous section, was transformed from MNI space to individual space as follows. First, the T_1-weighted image was brain extracted and aligned with the MNI brain extracted image using an affine transformation in FLIRT. Second, a nonlinear transformation (FNIRT) was used to generate a transformation between individual subject space and common space. Finally, the transformation from T_1 to MNI space was inverted and the NM SN masks were transformed to T_1 subject space. This process is shown in Figure 3B.

For each individual subject, the FA map was registered to the brain extracted T_1-weighted image and transformed to T_1-space using FLIRT, and the transformation matrix was saved. After this transformation, there was no discernible difference between the location of white matter tracts in the T_1-weighted image and those in the susceptibility distortion corrected FA map. Finally, the saved transformation matrix from T_1 weighted image space to diffusion space was applied to the NM SN masks to transform them from T_1-space to diffusion space [Li et al., 2012a,2012b,2013].

Rostral and Caudal SN Masks

The NM SN mask was divided into rostral (half of the mask) and caudal (half the mask) portions in MNI space to assess regional effects of PD in the SN. Both regions were transformed into the image spaces of individual subjects. In each region, average MD, average FA, and overlap with the hypointense SN were calculated.

Hypointense SN Mask

In most published studies, the SN was defined as the hypointense region between the cerebral peduncle and red nucleus in $b = 0$ images. This region, referred to as the hypointense SN here, was found using the procedure described below. In the $b = 0$ image of each subject, the SN was identified as the hypointense region between the cerebral peduncle and red nucleus. A mask incorporating this area was drawn by hand on the $b = 0$ image by J.L., similarly as in Schwarz et al. [2013]. J.L. was blinded to the status of each subject during this procedure. Diffusion metrics in this region were calculated for both subject groups and compared between them.

Overlap

Increased iron deposition in the SNpc is seen in histological studies [Dexter et al., 1987, 1991; Wypijewska et al., 2010]. One effect of this deposition is increased hypointensity in SNpc. The overlap between NM SN and T2w hypointense SN, defined below, offers a nonquantitative means to evaluate this deposition in NM SN.

$$\text{Overlap} = \frac{\text{Volume}\ (SN_{NM} \cap SN_{hypointense})}{\text{Volume}\ (SN_{NM})} \quad (1)$$

where SN_{NM} and $SN_{hypointense}$ denote the NM SN and T2w hypointense SN volumes, respectively.

Statistical Analysis

Statistical analyses were performed using SPSS version 22 (IBM SPSS Statistics, Chicago, IL). Quantitative data were expressed as mean ± standard deviation. A one-tailed *t*-test with a significance level of $P = 0.05$ was used for group comparisons. Correlations were performed between individual DTI measures, FA and MD, respectively, with UPDRS-III motor score and MOCA score, respectively. The correlation was considered to be significant if $P < 0.05$.

RESULTS

Demographic and clinical data of our subjects were summarized in Table I. There were statistically significant differences between PD and control groups in age. This factor was controlled for in all comparisons and correlations between groups.

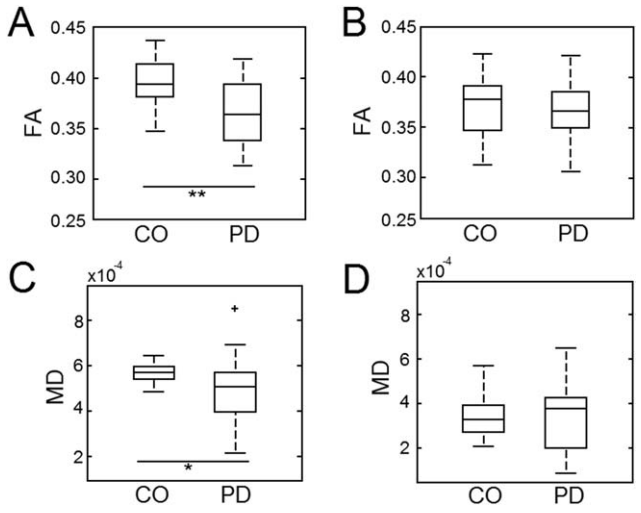

Figure 4.

Comparison of FA and MD in NM and T2w SN volumes. Box plots illustrating the mean FA for PD and CO groups in NM and T2w SN volumes are shown in (**A**) and (**B**), respectively. (**C**) and (**D**) display box plots illustrating the mean MD in NM and T2w SN volumes for PD and CO groups. In A and C, * and ** denote significance at the $P = 0.05$ and $P = 0.001$ levels, respectively.

Comparison of FA in NM and T2w Masks

A comparison of the relative positions for the NM and T2w SN volumes is shown in Figure 2. Mean FA values for the NM SN were lower in the PD group than in the control group (PD: 0.36 ± 0.03; Control: 0.39 ± 0.02; $P = 0.001$). In contrast, no statistically significant difference in mean FA was seen in the T2w SN volume (PD: 0.36 ± 0.03; control: 0.37 ± 0.03; $P = 0.36$). In addition, the average MD exhibited no statistically significant difference between the two groups in the SN for the T2w SN volume (PD: 3.43×10^{-4} mm^2/s $\pm$ 1.53×10^{-4} mm^2/s; control: 3.39×10^{-4} mm^2/s $\pm$ 9.40×10^{-5} mm^2/s; $P = 0.43$), while a statistically significant difference was seen in mean MD between PD and control groups for the NM SN (PD: 4.88×10^{-4} mm^2/s $\pm$ 1.46×10^{-4} mm^2/s; control: 5.73×10^{-4} mm^2/s $\pm$ 4.56×10^{-5} mm^2/s; $P = 0.01$). These results are summarized in Figure 4.

Rostral and Caudal Comparison Within NM Mask

The NM SN in MNI space was subdivided into rostral and caudal portions as shown in Figure 5, and both regions were transformed into the imaging spaces of individual subjects. Interestingly, disease effects are greater in the rostral portions of the NM SN when compared with the caudal portion of the mask. The mean FA in the caudal mask for the PD and control groups was 0.36 ± 0.04 and 0.39 ± 0.03 ($P = 0.01$), respectively, while the mean FA in the rostral portion of the NM SN was 0.37 ± 0.03 and 0.40 ± 0.02 ($P = 0.001$) for the PD and control groups, respectively. A significant difference was seen in the mean MD between PD and control groups for the caudal (PD: 4.51×10^{-4} mm^2/s $\pm$ 1.53×10^{-4} mm^2/s; control: 5.29×10^{-4} mm^2/s $\pm$ 6.30×10^{-5} mm^2/s; $P = 0.03$) and rostral portions (PD: 5.40×10^{-4} mm^2/s $\pm$ 1.53×10^{-4} mm^2/s; control: 6.20×10^{-4} mm^2/s $\pm$ 5.85×10^{-5} mm^2/s; $P = 0.001$) of the NM SN. These results are shown in Figure 5.

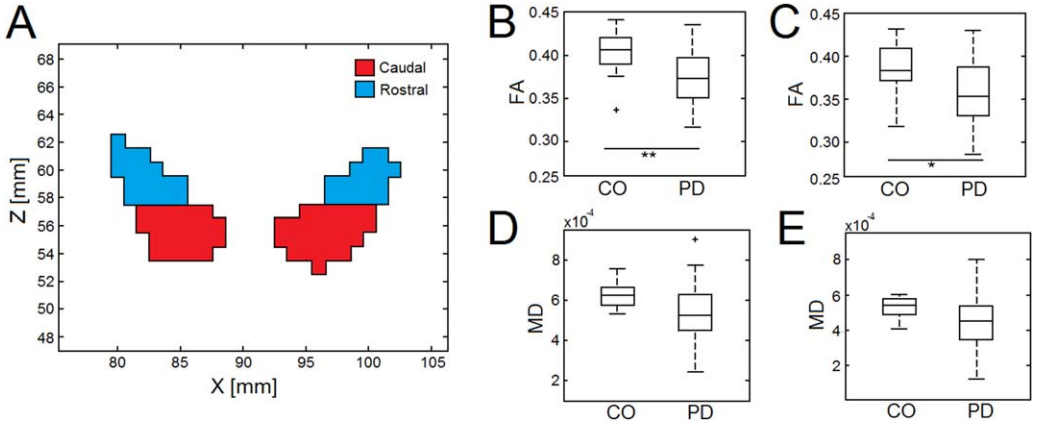

Figure 5.

Comparison of FA and MD in caudal and rostral portions of the NM SN. The choice of caudal and rostral sections of the NM SN is shown in (**A**). Box plots illustrating the mean FA for PD and CO groups in rostral and caudal regions of the NM SN are shown in (**B**) and (**C**), respectively. (**D**) and (**E**) display box plots illustrating the mean MD in rostral and caudal sections of the NM SN for PD and CO groups. In (A) and (C), * and ** denote significance at the $P = 0.05$ and $P = 0.001$ levels, respectively. [Color figure can be viewed in the online issue, which is available at wileyonlinelibrary.com.]

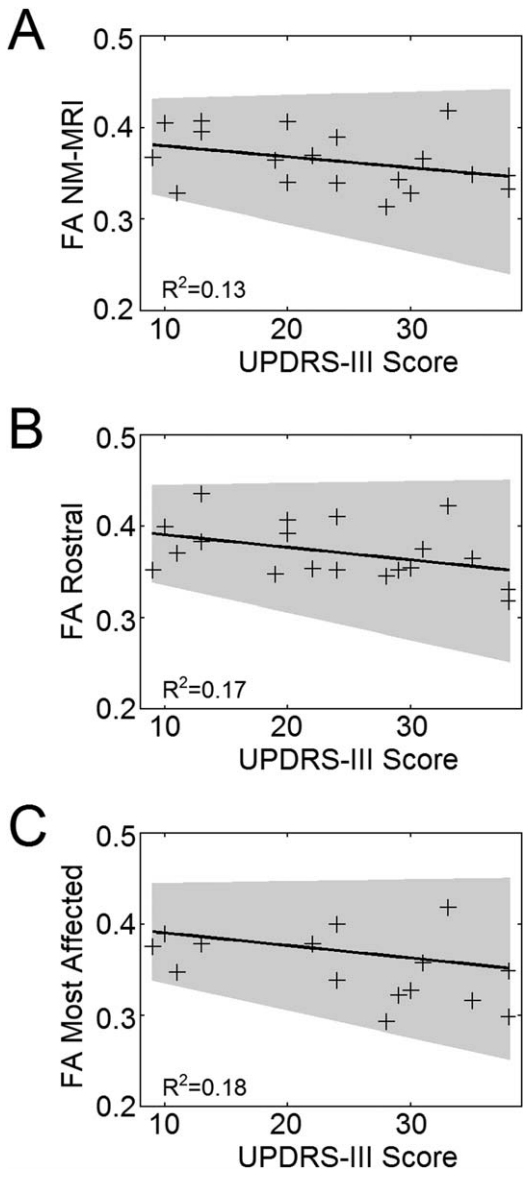

Figure 6.
Correlation between UPDRS-III score and FA in (**A**) the NM SN (A), (**B**) rostral portion of the NM SN, and (**C**) the NM SN contralateral to the more affected side. The gray area in each plot shows the 95% confidence interval.

UPDRS Correlation and Lateralization Analysis

No statistically significant correlation was seen between MD and UPDRS-III score in any SN volume (NM SN, T2w, rostral and caudal portions of NM SN). The FA in the NM SN showed a moderate correlation with UPDRS-III score ($R^2 = 0.13$; $P = 0.06$), as did FA in the rostral portion of the NM SN ($R^2 = 0.17$; $P = 0.04$). These correlations are shown in Figure 6A,B, respectively. No statistically significant correlation was seen between FA and UPDRS-III score in the other SN volumes (NM SN, T2w, caudal portions of NM SN). Furthermore, no significant correlation was seen between either mean MD or mean FA and MOCA in any SN volume.

Lateralized UPDRS-III sub-cores were summed, and the side with a higher summed score was set as the side more affected by PD. In the SN volume contralateral to the more affected side, the PD group had a lower FA than the control group (PD: 0.36 ± 0.03; CO: 0.41 ± 0.03; $P < 10^{-4}$). In addition, SN degeneration is asymmetric in the NM SN. Specifically, greater disease effects were seen in the FA in the rostral portion of the SN on the side contralateral to the more affected than the other side ($P = 0.03$). FA in the more affected side and total UPDRS-III score were moderately correlated ($R^2 = 0.18$; $P = 0.10$), as shown in Figure 6C.

DISCUSSION

In this work, we defined SN ROIs using SN volumes from neuromelanin sensitive MRI and applied them to ascertain changes in FA and MD due to PD. For comparison, the DTI measures in ROIs defined based on T2w images were also analyzed. While no disease-related changes in FA and MD were found in the T2w SN ROIs, statistically significant changes in FA and MD between PD and control groups were detected in the NM SN ROIs. Interestingly, the rostral portion of the NM SN was found to have a larger disease-related effect than the caudal portion of the NM SN. In addition, in the rostral portion of the NM SN, the FA was lower on the side contralateral to the more affected side, consistent with disease laterality.

Localization of SN ROIs

Inconsistency in locations of ROIs used for the SN could account for the variability in results of previous DTI studies of PD [Aquino et al., 2014; Chan et al., 2007; Du et al., 2011; Menke et al., 2009; Peran et al., 2010; Schwarz et al., 2013; Vaillancourt et al., 2009]. The study by Vaillancourt, et al. exhibited the biggest effect size in PD related changes in the SN [Vaillancourt et al., 2009]. In that study, ROIs were placed in the hypointense area in the slice inferior to the most inferior extent of the red nucleus. Although an accurate comparison of the volumes between the Vaillancourt study and the present work is difficult given the inconsistency in spatial location between T2w and NM SN volumes [Langley et al., 2015], the ROIs used in the Vaillancourt study are located in a similar anatomical position as the intersection of the rostral portion of the NM SN and the hypointense SN volume in the $b = 0$ image. A similarly sized disease effect is seen in the rostral portion of the NM SN in the present work.

Increased iron deposition in the SN for PD patients, and associated hypointensity, adds further variability to the definition of ROIs based on T2w images since increased

hypointense volume is not present in all subjects with PD. This is illustrated in Figure 1 where a slice 4 mm (or two slices) inferior to the most inferior extent of the red nucleus for two subjects from the PD group is shown. In one subject, in the slices shown in Figure 1a,b, additional hypointensity is seen and would be included in the SN volume while there is no hypointense signal in the same region for another subject (shown in Fig. 1c,d). The SN volume from neuromelanin-sensitive MRI includes this region for both subjects. If the $b = 0$ image, which has similar contrast characteristics as T2w, was used to draw the ROI, the NM SN in Figure 1d would not be included in the analysis as it is not within the hypointense region.

The inconsistency in the location and volume of SN ROIs, as shown in the $b = 0$ image, could explain the discrepancy between studies showing significant FA and MD changes in the SN of PD patients [Chan et al., 2007; Du et al., 2011; Peran et al., 2010; Vaillancourt et al., 2009] and those showing no PD related effects [Aquino et al., 2014; Menke et al., 2009; Schwarz et al., 2013]. These studies used a similar definition for SN ROIs as Vaillancourt et al. [2009]. However, as shown in Figure 1, PD patients in these studies with less iron deposition and less hypointensity in the $b = 0$ image could appear to have a smaller disease effect in DTI measures if the ROIs were determined by the T2w SN volume, which was found to exhibit no disease-related changes in DTI measures in this study.

Effect of Iron on Diffusion Measures

We observed that the hypointense region of the SN in the $b = 0$ image extended outside the T2w SN volume in many PD patients and this region always extends from the border of the T2w and NM SN volumes to interior portions of the NM SN. The mean overlap between the hypointense region and the NM SN was found to be approximately 43% for the PD group as compared with approximately 20% for the control group. The hypointensity could be due to accumulation of iron in these areas since multiple T2w imaging studies have shown an increase in iron content in the SN for subjects with PD when compared with controls [Du et al., 2011; Lotfipour et al., 2012; Martin et al., 2008]. In addition, it has been shown that diffusion-weighted MRI volumes are sensitive to iron [Fujiwara et al., 2014] and increased iron content might explain the higher sensitivity to PD related changes in the rostral volume. In this volume, any effects from iron would be combined with changes reflected in the underlying tissue due to pathology since the loss of MR signal from increased iron deposition has been found to decrease the FA in regions with high and intermediate FA values [Landman et al., 2008].

In $b = 0$ images of PD subjects, less hypointense signal was observed in the region corresponding to the caudal portion of the NM SN and, although iron related measures (such as R_2*) were not collected in this study, we can infer lower concentrations of iron in the caudal portions of the NM SN from the lack of hypointensity in the $b = 0$ image. Specifically, 55% of the rostral portion of the NM SN showed hypointensity in PD patients while approximately 10% overlap was seen between the caudal portion exhibited hypointense signal. Given this, the differences in FA seen in the caudal portion could be primarily due to changes in the underlying tissue and not a combination of diffusivity and iron accumulation as is likely the case in the rostral portion of the NM SN. However, future studies comparing iron sensitive measures (such as R_2*) and diffusion measures in the caudal and rostral NM SN regions are needed to verify this hypothesis.

In controls, approximately 20% of the NM SN shows hypointensity while significantly more hypointensity is seen in NM SN of PD patients (~50% of NM SN shows hypointensity). Importantly, the zone within the NM SN volume that exhibits hypointensity in PD is located in the lateral and ventral portions of the NM SN. This correlates with the well described histopathology of PD which is characterized by degeneration of melanized dopamine neurons in the lateral ventral tier of SNpc [Damier et al., 1999; Fearnley and Lees, 1991; Hassler, 1938]. Microglia are activated when neuromelanin containing neurons die and neuromelanin granules are released into the extracellular space. Because neuromelanin granules are insoluble they may potentiate a chronic state of microglial activation and neuroinflammation. As these granules are phagocytosed and degraded, the toxic species sequestered in neuromelanin, including oxidizing species of iron, are released and further drive the neurodegeneration process [Block et al., 2007; Zecca et al., 2003, 2015]. This local inflammation and release of sequestered iron provides a compelling potential explanation and link to PD biology for the increased iron signal ($b = 0$ hypointensity) seen within SNpc (as defined by neuromelanin-sensitive MRI) in PD subjects as compared with controls. Furthermore, the accumulation of paramagnetic iron released by the neuroinflammatory process in the lateral ventral portion of the NM SN would explain our findings that both FA and MD are decreased in PD as compared with controls as explained above.

Asymmetric Degeneration Patterns

Motor symptoms generally start on one side of the body and then progress to the other side [Hoehn and Yahr, 1967]. In the SNpc, this asymmetry is present in the form of dopaminergic neuronal loss in the SNpc contralateral to side more affected by PD [Kempster et al., 1989]. In the current work, we found a similar pattern of asymmetric degeneration. Specifically, the NM SN contralateral to the side more affected by PD was shown to have a lower FA than the less affected side in PD patients.

Age-Specific and Standardized ROIs

For analyses performed in the presented study, NM SN masks were derived from a cohort of young healthy controls. These masks were used to define ROIs applied in the FA and MD analysis. Similarly, T2w SN masks can be derived in a cohort of controls and transformed to standard space. However, iron concentration in the T2w SN volume is known to vary with age [Bilgic et al., 2012; Haacke et al., 2007]. Hence, the size of the T2w SN volume could be age dependent and future studies should take this variability into account by developing age-specific T2w SN masks. In addition, neuromelanin concentration in the locus coeruleus has been found to vary with age [Shibata et al., 2006], and it is possible that neuromelanin concentration in the SNpc is also dependent on age. However, no imaging study has explored this possibility in the SNpc.

In this study, ROIs used for the SN were defined from T2w and NM SN masks generated from a group of young healthy controls. Individual NM SN masks could be used in lieu of these masks. However, postmortem studies have found a loss of dopaminergic neurons in caudal and lateral portions of the SNpc for subjects with PD [Damier et al., 1999; Fearnley and Lees, 1991]. A reduction in neuromelanin sensitive contrast in PD is expected, and NM SN mask from PD patients may not include the entire NM SN mask derived from the controls The use of population masks, as derived from controls, allows for the examination of MD and FA in a more standardized and unbiased manner.

The spatial location of SN ROIs varies between studies and has been an impediment to the development of diffusion-related PD biomarkers [Schwarz et al., 2013]. Consistent placement of SN ROIs can be achieved by defining ROIs in standard space and transforming them to individual subject space. The use of SN ROIs defined in standard space allows for diffusion data in different studies to be analyzed with similar ROIs.

CONCLUSION

In summary, we have presented an approach to ascertain PD related changes more consistently in the SN by utilizing standardized SN ROIs. Mean FA and MD values in SN ROIs defined using neuromelanin-sensitive MRI were lower in PD subjects when compared with controls but no difference was seen in T2w SN volumes. Furthermore, the disease effects in the rostral portion of the NM SN were larger than those in the caudal portion of the NM SN, which could be due to a combination of disease effects and iron accumulation in the rostral portion. Finally, we found asymmetry in the mean FA of the rostral portion of the NM SN, which was related to the side more affected by PD.

REFERENCES

Alexander AL, Tsuruda JS, Parker DL (1997): Elimination of eddy current artifacts in diffusion-weighted echo-planar images: The use of bipolar gradients. Magn Reson Med 38: 1016–1021.

Andersson JL, Skare S, Ashburner J (2003): How to correct susceptibility distortions in spin-echo echo-planar images: application to diffusion tensor imaging. Neuroimage 20:870–888.

Aquino D, Contarino V, Albanese A, Minati L, Farina L, Grisoli M, Elia A, Bruzzone MG, Chiapparini L (2014): Substantia nigra in Parkinson's disease: A multimodal MRI comparison between early and advanced stages of the disease. Neurol Sci 35:753–758.

Bilgic B, Pfefferbaum A, Rohlfing T, Sullivan EV, Adalsteinsson E (2012): MRI estimates of brain iron concentration in normal aging using quantitative susceptibility mapping. Neuroimage 59:2625–2635.

Block ML, Zecca L, Hong JS (2007): Microglia-mediated neurotoxicity: Uncovering the molecular mechanisms. Nat Rev Neurosci 8:57–69.

Castellanos G, Fernandez-Seara MA, Lorenzo-Betancor O, Ortega-Cubero S, Puigvert M, Uranga J, Vidorreta M, Irigoyen J, Lorenzo E, Munoz-Barrutia A, Ortiz-de-Solorzano C, Pastor P, Pastor MA (2015): Automated neuromelanin imaging as a diagnostic biomarker for Parkinson's disease. Mov Disord 30: 945–952.

Chan LL, Rumpel H, Yap K, Lee E, Loo HV, Ho GL, Fook-Chong S, Yuen Y, Tan EK (2007): Case control study of diffusion tensor imaging in Parkinson's disease. J Neurol Neurosurg Psychiatry 78:1383–1386.

Chen X, Huddleston DE, Langley J, Ahn S, Barnum CJ, Factor SA, Levey AI, Hu X (2014): Simultaneous imaging of locus coeruleus and substantia nigra with a quantitative neuromelanin MRI approach. Magn Reson Imaging 32:1301–1306.

Damier P, Hirsch EC, Agid Y, Graybiel AM (1999): The substantia nigra of the human brain. II. Patterns of loss of dopamine-containing neurons in Parkinson's disease. Brain 122:1437–1448.

Dexter DT, Carayon A, Javoy-Agid F, Agid Y, Wells FR, Daniel SE, Lees AJ, Jenner P, Marsden CD (1991): Alterations in the levels of iron, ferritin and other trace metals in Parkinson's disease and other neurodegenerative diseases affecting the basal ganglia. Brain 114:1953–1975.

Dexter DT, Wells FR, Agid F, Agid Y, Lees AJ, Jenner P, Marsden CD (1987): Increased nigral iron content in postmortem Parkinsonian brain. Lancet 2:1219–20.

Du G, Lewis MM, Styner M, Shaffer ML, Sen S, Yang QX, Huang X (2011): Combined R2* and diffusion tensor imaging changes in the substantia nigra in Parkinson's disease. Mov Disord 26: 1627–1632.

Fearnley JM, Lees AJ (1991): Ageing and Parkinson's disease: Substantia nigra regional selectivity. Brain 114:2283–2301.

Fujiwara S, Uhrig L, Amadon A, Jarraya B, Le Bihan D (2014): Quantification of iron in the non-human primate brain with diffusion-weighted magnetic resonance imaging. Neuroimage 102:789–797.

Haacke EM, Ayaz M, Khan A, Manova ES, Krishnamurthy B, Gollapalli L, Ciulla C, Kim I, Petersen F, Kirsch W (2007): Establishing a baseline phase behavior in magnetic resonance imaging to determine normal vs. abnormal iron content in the brain. J Magn Reson Imaging 26:256–264.

Hassler R (1938): Zur Pathologie der Paralysis agitains und des postenzephalitischen Parkinsonismus. J Psychol Neurol 48: 387–476.

He N, Ling H, Ding B, Huang J, Zhang Y, Zhang Z, Liu C, Chen K, Yan F (2015): Region-specific disturbed iron distribution in early idiopathic Parkinson's disease measured by quantitative susceptibility mapping. Hum Brain Mapp 36:4407–4420.

Hoehn MM, Yahr MD (1967): Parkinsonism: Onset, progression, and mortality. Neurology 17:427–442.

Jenkinson M, Bannister P, Brady M, Smith S (2002): Improved optimization for the robust and accurate linear registration and motion correction of brain images. Neuroimage 17: 825–841.

Jenkinson M, Smith S (2001): A global optimisation method for robust affine registration of brain images. Med Image Anal 5: 143–156.

Kashihara K, Shinya T, Higaki F (2011): Neuromelanin magnetic resonance imaging of nigral volume loss in patients with Parkinson's disease. J Clin Neurosci 18:1093–1096.

Kempster PA, Gibb WR, Stern GM, Lees AJ (1989): Asymmetry of substantia nigra neuronal loss in Parkinson's disease and its relevance to the mechanism of levodopa related motor fluctuations. J Neurol Neurosurg Psychiatry 52:72–76.

Keren NI, Lozar CT, Harris KC, Morgan PS, Eckert MA (2009): In vivo mapping of the human locus coeruleus. Neuroimage 47: 1261–1267.

Keren NI, Taheri S, Vazey EM, Morgan PS, Granholm AC, Aston-Jones GS, Eckert MA (2015): Histologic validation of locus coeruleus MRI contrast in post-mortem tissue. Neuroimage 113:235–245.

Kitao S, Matsusue E, Fujii S, Miyoshi F, Kaminou T, Kato S, Ito H, Ogawa T (2013): Correlation between pathology and neuromelanin MR imaging in Parkinson's disease and dementia with Lewy bodies. Neuroradiology 55:947–953.

Landman BA, Farrell JA, Huang H, Prince JL, Mori S (2008): Diffusion tensor imaging at low SNR: Nonmonotonic behaviors of tensor contrasts. Magn Reson Imaging 26:790–800.

Langley J, Huddleston D, Chen X, Sedlacik J, Zachariah N, Hu X (2015): A multicontrast approach for comprehensive imaging of substantia nigra. Neuroimage 112:7–13.

Li L, Hu X, Preuss TM, Glasser MF, Damen FW, Qiu Y, Rilling J (2013): Mapping putative hubs in human, chimpanzee and rhesus macaque connectomes via diffusion tractography. Neuroimage 80:462–474.

Li L, Rilling JK, Preuss TM, Glasser MF, Damen FW, Hu X (2012a): Quantitative assessment of a framework for creating anatomical brain networks via global tractography. Neuroimage 61:1017–1030.

Li L, Rilling JK, Preuss TM, Glasser MF, Hu X (2012b): The effects of connection reconstruction method on the interregional connectivity of brain networks via diffusion tractography. Hum Brain Mapp 33:1894–1913.

Lotfipour AK, Wharton S, Schwarz ST, Gontu V, Schafer A, Peters AM, Bowtell RW, Auer DP, Gowland PA, Bajaj NP (2012): High resolution magnetic susceptibility mapping of the substantia nigra in Parkinson's disease. J Magn Reson Imaging 35: 48–55.

Martin WR, Wieler M, Gee M (2008): Midbrain iron content in early Parkinson disease: A potential biomarker of disease status. Neurology 70:1411–1417.

Matsuura K, Maeda M, Yata K, Ichiba Y, Yamaguchi T, Kanamaru K, Tomimoto H (2013): Neuromelanin magnetic resonance imaging in Parkinson's disease and multiple system atrophy. Eur Neurol 70:70–77.

Menke RA, Scholz J, Miller KL, Deoni S, Jbabdi S, Matthews PM, Zarei M (2009): MRI characteristics of the substantia nigra in Parkinson's disease: A combined quantitative T1 and DTI study. Neuroimage 47:435–441.

Ogisu K, Kudo K, Sasaki M, Sakushima K, Yabe I, Sasaki H, Terae S, Nakanishi M, Shirato H (2013): 3D neuromelanin-sensitive magnetic resonance imaging with semi-automated volume measurement of the substantia nigra pars compacta for diagnosis of Parkinson's disease. Neuroradiology 55: 719–724.

Peran P, Cherubini A, Assogna F, Piras F, Quattrocchi C, Peppe A, Celsis P, Rascol O, Demonet JF, Stefani A, Pierantozzi M, Pontieri FE, Caltagirone C, Spalletta G, Sabatini U (2010): Magnetic resonance imaging markers of Parkinson's disease nigrostriatal signature. Brain 133:3423–3433.

Reimao S, Pita Lobo P, Neutel D, Correia Guedes L, Coelho M, Rosa MM, Ferreira J, Abreu D, Goncalves N, Morgado C, Nunes RG, Campos J, Ferreira JJ (2015a): Substantia nigra neuromelanin magnetic resonance imaging in de novo Parkinson's disease patients. Eur J Neurol 22:540–546.

Reimao S, Pita Lobo P, Neutel D, Guedes LC, Coelho M, Rosa MM, Azevedo P, Ferreira J, Abreu D, Goncalves N, Nunes RG, Campos J, Ferreira JJ (2015b): Substantia nigra neuromelanin-MR imaging differentiates essential tremor from Parkinson's disease. Mov Disord 30:953–959.

Rossi M, Ruottinen H, Elovaara I, Ryymin P, Soimakallio S, Eskola H, Dastidar P (2010): Brain iron deposition and sequence characteristics in Parkinsonism: comparison of SWI, T(2)* maps, T(2)-weighted-, and FLAIR-SPACE. Invest Radiol 45:795–802.

Sasaki M, Shibata E, Tohyama K, Takahashi J, Otsuka K, Tsuchiya K, Takahashi S, Ehara S, Terayama Y, Sakai A (2006): Neuromelanin magnetic resonance imaging of locus ceruleus and substantia nigra in Parkinson's disease. Neuroreport 17: 1215–1218.

Schwarz ST, Abaei M, Gontu V, Morgan PS, Bajaj N, Auer DP (2013): Diffusion tensor imaging of nigral degeneration in Parkinson's disease: A region-of-interest and voxel-based study at 3 T and systematic review with meta-analysis. Neuroimage Clin 3:481–488.

Shibata E, Sasaki M, Tohyama K, Kanbara Y, Otsuka K, Ehara S, Sakai A (2006): Age-related changes in locus ceruleus on neuromelanin magnetic resonance imaging at 3 Tesla. Magn Reson Med Sci 5:197–200.

Smith SM (2002): Fast robust automated brain extraction. Hum Brain Mapp 17:143–155.

Smith SM, Jenkinson M, Woolrich MW, Beckmann CF, Behrens TE, Johansen-Berg H, Bannister PR, De Luca M, Drobnjak I, Flitney DE, Niazy RK, Saunders J, Vickers J, Zhang Y, De Stefano N, Brady JM, Matthews PM (2004): Advances in functional and structural MR image analysis and implementation as FSL. Neuroimage 23(Suppl 1):S208–S219.

Vaillancourt DE, Spraker MB, Prodoehl J, Abraham I, Corcos DM, Zhou XJ, Comella CL, Little DM (2009): High-resolution diffusion tensor imaging in the substantia nigra of de novo Parkinson disease. Neurology 72:1378–1384.

Woolrich MW, Jbabdi S, Patenaude B, Chappell M, Makni S, Behrens T, Beckmann C, Jenkinson M, Smith SM (2009): Bayesian analysis of neuroimaging data in FSL. Neuroimage 45: S173–S186.

Wypijewska A, Galazka-Friedman J, Bauminger ER, Wszolek ZK, Schweitzer KJ, Dickson DW, Jaklewicz A, Elbaum D, Friedman A (2010): Iron and reactive oxygen species activity in parkinsonian substantia nigra. Park Relat Disord 16:329–333.

Zecca L, Zucca FA, Wilms H, Sulzer D (2003): Neuromelanin of the substantia nigra: A neuronal black hole with protective and toxic characteristics. Trends Neurosci 26: 578–580.

Zucca FA, Segura-Aguilar J, Ferrari E, Munoz P, Paris I, Sulzer D, Sarna T, Casella L, Zecca L (2015): Interactions of iron, dopamine and neuromelanin pathways in brain aging and Parkinson's disease. Prog Neurobiol. DOI: 10.1016/j.pneurobio.2015.09.012.